

RESEARCH ARTICLE

Characterization of amine proton exchange for analyzing the specificity and intensity of the CEST effect: from humans to fish

Felizitas C. Wermter¹ | Christian Bock²  | Wolfgang Dreher¹

¹Department of Chemistry, in-vivo-MR group, University Bremen, Bremen, Germany

²Integrative Ecophysiology, Alfred Wegener Institute Helmholtz Centre for Polar and Marine Research, Bremerhaven, Germany

Correspondence

F.C. Wermter, University Bremen, Department of Chemistry, in-vivo-MR group, 28359 Bremen, Germany.
Email: fwermt@uni-bremen.de

Funding information

Deutsche Forschungsgemeinschaft, Grant/Award Numbers: DR298/13-1, DR298/13-2, BO2467/4-1, BO2467/4-2, WE6575/1-1

Chemical exchange saturation transfer (CEST) at about 2.8 ppm downfield from water is characterized besides other compounds by exchanging amine protons of relatively high concentration amino acids and is determined by several physiological (pH , T) and experimental (B_0 , B_1 , t_{sat}) parameters. Although the weighting of the CEST effect observed *in vivo* can be attributed mainly to one compound depending on the organism and organ, there are still several other amino acids, proteins and molecules that also contribute. These contributions in turn exhibit dependences and thus can lead to possible misinterpretation of the measured changes in the CEST effect. With this in mind, this work aimed to determine the exchange rates of six important amino acids as a function of pH and temperature, and thus to create multi-pool models that allow the accurate analysis of the CEST effect concerning different physiological and experimental parameters for a wide variety of organisms. The results show that small changes in the above parameters have a significant impact on the CEST effect at about 2.8 ppm for the chosen organisms, i.e. the human brain (37 °C) and the brain of polar cod (1.5 °C), furthermore, the specificity of the CEST effect observed *in vivo* can be significantly affected. Based on the exchange rates $k_{sw}(pH, T)$ determined for six metabolites in this study, it is possible to optimize the intensity and the specificity for the CEST effect of amino acids at about 2.8 ppm for different organisms with their specific physiological characteristics. By adjusting experimental parameters accordingly, this optimization will help to avoid possible misinterpretations of CEST measurements. Furthermore, the multi-pool models can be utilized to further optimize the saturation.

KEYWORDS

chemical exchange saturation transfer (CEST), exchange rate, pH, temperature

Abbreviations: Ala, alanine; APT, amide proton transfer; Asp, aspartate; B_0 , magnetic field; B_1 , saturation amplitude; CEST, chemical exchange saturation transfer; FISP, fast imaging with steady-state precession; GABA, γ -aminobutyric acid; Gln, glutamine; Glu, glutamate; k_{sw} , exchange rate from solute to water; MTC, magnetization transfer contrast; pH_i , intracellular pH; PLL, poly-L-lysine; SAR, specific absorption rate; T, temperature; Tau, taurine; t_{sat} , saturation time; WEX spectroscopy, water-exchange filter spectroscopy.

This is an open access article under the terms of the Creative Commons Attribution License, which permits use, distribution and reproduction in any medium, provided the original work is properly cited.

© 2021 The Authors. *NMR in Biomedicine* published by John Wiley & Sons Ltd.

1 | INTRODUCTION

Chemical exchange saturation transfer (CEST) imaging enables the indirect detection of endogenous and exogenous compounds such as amino acids, proteins and other molecules with exchangeable protons exhibiting, e.g., amide (-NH), amine (-NH₂) or hydroxyl (-OH) groups. The principle of CEST is the change of the NMR signal of water after the selective saturation of magnetization of the exchangeable protons. The CEST effect is mainly determined by the concentration of compounds and the exchange rate (k_{sw}) between the labile bound protons from these and water, whereby k_{sw} in turn is determined by the chemical structure and physiological parameters. Furthermore, the ratio of k_{sw} and the chemical shift difference ($\Delta\omega$) between the resonances of water and the exchangeable protons of the compound determines the intensity of the expected CEST effect. The different exchange regimes are defined as slow if $\frac{k_{sw}}{\Delta\omega} \ll 1$, intermediate if $\frac{k_{sw}}{\Delta\omega} \sim 1$, and fast if $\frac{k_{sw}}{\Delta\omega} \gg 1$.¹ CEST imaging is mostly sensitive to the slow- to intermediate-exchange regime defined by $k_{sw} [s^{-1}] \leq \Delta\omega [\frac{rad}{s}]$ and for this reason is dependent on the field strength used. Therefore, a trend in medical research is to focus on higher magnetic fields (B_0) for CEST imaging.²

The CEST effect, being observed after saturation at about 2.8 ppm downfield from water is, among other things, largely determined by exchangeable amine protons of relatively highly concentrated amino acids, which play an important role in the metabolism of the central nervous system of vertebrates and fulfil a variety of specific functions.³ For example, they form the basis for the synthesis of proteins and nucleic acids or are involved in energy metabolism and neurotransmission. Their non-specific functions include, e.g., their involvement in osmoregulation. Besides glutamate (Glu), whose CEST effect has already been established in preclinical research,⁴⁻⁹ several amino acids play important roles in the metabolism of the central nervous system. Due to their function and concentration, the amino acids alanine (Ala), γ -aminobutyric acid (GABA), aspartate (Asp), glutamine (Gln) and taurine (Tau) are also particularly relevant for the consideration of the total CEST effect at about 2.8 ppm. Lee *et al.* published the examination of CEST effects from endogenous agents that are typically found in biological tissues and organs, e.g. Glu, Gln, GABA and Tau, at different pH conditions and B_0 values.¹⁰ In combination with ¹H NMR spectra, these CEST effects have been analyzed in consideration of the k_{sw} , chemical shifts and acidities of the labile protons.¹⁰ Khlebnikov *et al.* have also studied the most important metabolites that contribute to the CEST effect in the human brain.¹¹ Their exchange rates were investigated at physiological pH and 37 °C. Additionally, the contributions of these metabolites to the total CEST effect were determined at different field strengths. However, the k_{sw} as well as their pH and temperature (T) dependences for the metabolites were only investigated selectively and not for a wider range of values,^{4,10-13} which does not allow the exchange rate to be determined as a function of pH and temperature ($k_{sw}(pH, T)$).

Although the *in vivo* observed CEST effect is often dominated by one compound, others contribute as well. Cai *et al.* could show that 70-75% of the CEST effect observed *in vivo* in the human brain is determined by Glu, while 25-30% remained from other products.⁴ However, these percentages may change depending on physiological (i.e. concentration, temperature and pH) and experimental parameters (i.e. B_0 , saturation amplitude (B_1) and saturation time (t_{sat})). Therefore, a determination of $k_{sw}(pH, T)$ will simplify both the analysis of CEST effects and the optimization of the pulse sequences used.¹⁴

There is a growing interest in alternative and non-endothermic animal models for *in vivo* studies (e.g. birds¹⁵ or fish¹⁶⁻²¹), which considerably extends the number of compounds of interest and the range of temperature and pH in which this methodology is applied. Recently, the application of the TauCEST effect allowed us to determine relative changes in intracellular pH (pH_i) in the brain of the polar cod (*Boreogadus saida*) due to changes in CO₂ concentrations under polar conditions *in vivo*.²² This is based on the exceptionally high Tau concentration in saltwater fish (about 20 mM in the brain of polar cod (*B. saida*)²³ and up to 65.7 mM in the brain of stingray (*Dasyatis sabina*)²⁴) compared with adult rodents (around 2 mM to 6-8 mM),²⁵⁻²⁸ due to their osmoregulatory function. This aspect, in combination with the body temperature of 1 °C, results in a contribution of Tau of about 65% to the observed total CEST effect in the physiological pH range *in vivo*.²² Even in conventional preclinical research, other physiological conditions can occur during the measurements, for example, due to temperature changes. Pyrexia and anesthesia without an external control system can cause changes between 32 and 40 °C even at a basal body temperature of 37 °C.²⁹ Furthermore, the specificity of the *in vivo* observed CEST effect changes due to changes in pH (e.g. hypercapnia, tumor tissue^{30,31}).

Against this background, the high dependence of the CEST effect on several physiological parameters may cause misinterpretations. Some methodological approaches have already been developed to eliminate or extract certain contributions to the CEST effect. Jones *et al.* developed a fast low- B_1 pulsed CEST acquisition with optimized pulse parameters to reduce the contributions from magnetization transfer contrast (MTC) and direct saturation to retain nearly the maximal amide proton transfer (APT) effect.³² This methodical approach utilized the fact that direct saturation width and MTC magnitude increase strongly with B_1 , while the effect of compounds with relative slowly exchanging protons as in APT only depends slightly on B_1 .

However, the amino acids have similar physical properties, including nearly identical resonance frequencies, which makes experimental separation considerably more difficult. This requires a more detailed analysis of these metabolites and the effect of physiological and experimental parameters. This work aimed to simulate and analyze as accurately as possible the intensity and specificity of the expected *in vivo* CEST effect of amino acids for different organisms and their corresponding body temperatures, based on a determination of $k_{sw}(pH, T)$ for six important brain metabolites. For the metabolites investigated in more detail, z-spectra and their corresponding asymmetry curves were determined experimentally for 36 combinations of pH values and temperatures. For the amino acids, which are particularly relevant for analyzing the total CEST effect at about 2.8 ppm, the exchange rates were determined by fitting the measured data with the Bloch-McConnell equation. Subsequently, the

maximum CEST effect was investigated as a function of the experimental parameters B_0 , B_1 and t_{sat} for the human brain as a representative of the clinical and preclinical research (37 °C body temperature) and for polar cod as an example for a new field of application (1.5 °C).

Finally, the intensity and specificity of the CEST effect are analyzed as a function of temperature and pH value using optimal experimental parameters for both organisms.

2 | EXPERIMENTAL

2.1 | Pulse sequence parameters

All NMR measurements were made on a 7 T animal scanner (BioSpec 70/20 USR, Bruker BioSpin, Ettlingen, Germany) equipped with a BGA-12S2 B_0 gradient system (maximum gradient strength 440 mT m⁻¹, rise time 130 μ s). A quadrature birdcage coil (72 mm inner diameter) was used both for RF excitations and signal detection.

To obtain sufficient B_0 homogeneity, FASTMAP (Fast Automatic Shimming Technique by Mapping Along Projections) was employed, ensuring line widths (full width at half maximum) of 8 Hz or less for the water signal.³³ CEST images were obtained as described before by Wermter *et al.* by applying a saturation module prior to fast imaging with steady-state precession (FISP) using centered phase encoding and the following sequence parameters: field of view 35 × 35 mm², matrix size 64 × 64, slice thickness 2 mm, flip angle 9°, repetition time $T_{R1} = 3.2$ ms, echo time $T_E = 1.6$ ms.¹³ Saturation was accomplished by a train of 12 rectangular pulses with an RF irradiation amplitude $B_1 = 5.87$ μ T, pulse width $t_p = 1$ s and inter-pulse delay $t_d = 50$ μ s. Z-spectra were obtained at 31 frequency offsets $\Delta\nu$ between -5 and 5 ppm. After acquiring each FISP image, the residual z-magnetization was destroyed by a 90° sech pulse. The repetition time between subsequent experiments was $T_{R2} = 15$ s. For normalization, fully relaxed images were acquired with an off-resonance frequency of about -17 ppm (5000 Hz) of the saturation pulse sufficient for *in vitro* measurements. To minimize the variables in the determination of exchange rates, the longitudinal relaxation times (T_1) of water were determined for each temperature and each series of measurements using a RARE (rapid acquisition with relaxation enhancement) sequence ($T_R = 5000$ ms, 3000 ms, 1500 ms, 800 ms, 400 ms, 227 ms).

2.2 | Phantom preparation

Phantoms were built to study the effect of pH and temperature on exchange rates of Ala, GABA, Asp, Gln, Glu and Tau. Each of the phantoms consisted of six NMR tubes filled with 10 mM metabolite solutions dissolved in phosphate-buffered saline (12 mM HPO₄²⁻, 0.1 M NaCl), titrated to different pH values of about 5.5, 6.0, 6.5, 7.0, 7.5 and 8.0. The sealed NMR tubes were then embedded in a 3% agarose solution. The agarose was mixed with filtered and deionized water, heated to boiling and then immersed in a water bath at 46 °C. After 15 min the agarose solution was filled into a 50 mL Falcon tube, into which the NMR tubes were inserted.^{13,34} The phantoms were wrapped with heating tubings connected to a circulation thermostat (Lauda Eco RE 630S, Lauda-Brinkmann, Delran, NJ) for measurements at defined temperatures (1-37 °C), while temperature measurements inside the magnet were performed with a two-point calibrated fiber-optical thermometer (Luxtron 504, Polytec, Waldheim, Germany).

2.3 | Methods of data analysis

The CEST images were analyzed by determining the mean signal intensities from different regions of interest in the tubes of the phantoms using ImageJ (Version 1.48v, US National Institutes of Health, Bethesda, MD). Further calculations and data fitting were done using programs written in Scilab (Version 6.0.1, Scilab Enterprises, Versailles, France). The signal minimum in the z-spectrum at the water signal was fitted to a Lorentzian line shape to correct for B_0 inhomogeneities.³⁵

The exchange rates and the transverse relaxation times (T_2) of water were determined by fitting the Bloch-McConnell equations,³⁶ modified for a two-pool chemical exchange, to the experimental data.^{13,37}

A saturation time of 12 s allowed us to postulate steady-state conditions. The set of coupled linear first-order homogenous differential equations for the two-pool case without algebraic simplifications was numerically solved using a Nelder-Mead algorithm.³⁸ Since the relaxation times of the metabolites are inconsequential to the fitting routine, these values were fixed to $T_{1m} = 1000$ ms and $T_{2m} = 100$ ms.^{36,39} For the amino acids, the chemical shift difference between the amine protons and water resonance was assumed to be 2.8 ppm for Ala, Asp, Gln and Tau,^{10,11,40} 3.0 ppm for Glu^{4,41} and 2.75 ppm for GABA.¹² Despite small shifts in peak position due to changes in pH and temperature, all chemical shifts reported here were assumed to be constant to maintain consistency.⁴ All phantom experiments were repeated five times.

2.4 | Data modelling

The pH dependence of the proton exchange rate in aqueous solutions can be defined as^{14,42,43}

$$k_{\text{sw}} = k_{\text{a}} [\text{H}_3\text{O}^+] + k_{\text{b}} [\text{OH}^-] + k_{\text{buffer}} \quad (1)$$

where k_{a} , k_{b} and k_{buffer} denote the exchange rate of acid-catalyzed exchange, base-catalyzed exchange and other contributions, e.g. from the buffer, respectively.

The Arrhenius equation describes the temperature dependence of exchange rates⁴⁴:

$$k = A \cdot e^{-E_{\text{A}}/RT} \quad (2)$$

with A being a characteristic constant for the chemical process, E_{A} the activation energy, $R = 8.314 \text{ J (mol K)}^{-1}$ the general gas constant and T the absolute temperature.

Assuming that the amine proton exchanges of amino acids are predominantly base catalyzed and buffer catalyzed, it can be assumed for each temperature that^{14,45}

$$k_{\text{sw}}(\text{pH}, T) = k_{\text{b}}(T) [\text{OH}^-] \times 10^{\text{pH} - \text{pK}_{\text{w}}(T)} + k_{\text{buffer}}. \quad (3)$$

The temperature dependence of the pK of water ($\text{pK}_{\text{w}}(T)$) is given by the solution of the Van't Hoff equation⁴⁶:

$$\text{pK}_{\text{w}}(T) = \text{pK}_{\text{w}}(T_0) - \left[\left(\frac{\Delta H_{\text{R}}^0}{R \ln 10} \right) (1/T_0 - 1/T) \right] \quad (4)$$

with the standard reaction enthalpy for the self-dissociation of water $\Delta H_{\text{R}}^0 = 55.84 \text{ kJ mol}^{-1}$ and a $\text{pK}_{\text{w}} = 14$ at $T_0 = 25^\circ\text{C} = 298.15 \text{ K}$.¹⁴ Thus $k_{\text{sw}}(\text{pH}, T)$ is given by

$$k_{\text{sw}}(\text{pH}, T) = k_{\text{base, eff}}(298.15 \text{ K}) * \left(e^{\left(\frac{E_{\text{A, base}}}{R} * \left(\frac{1}{298.15 \text{ K}} - \frac{1}{T} \right) \right)} * 10^{(\text{pH} - \text{pK})} + k_{\text{buffer, eff}}(298.15 \text{ K}) * \left(e^{\left(\frac{E_{\text{A, buffer}}}{R} * \left(\frac{1}{298.15 \text{ K}} - \frac{1}{T} \right) \right)} * 10^{(\text{pH} - \text{pK})} \right). \quad (5)$$

For the modeling of $k_{\text{sw}}(\text{pH}, T)$, only exchange rates below $22\,000 \text{ s}^{-1}$ and with a standard deviation of less than 10% were included, to ensure the validity of the data and the modeling.

2.5 | Simulations

Simulations were performed by numerically solving the Bloch-McConnell equations using the two-pool model. Additionally, for a multi-pool simulation, the model was extended according to Sun.³⁷ We solved the Bloch equations and calculated the spectra by using the 'ode' (ordinary differential equation) solver in Scilab.

The CEST asymmetry was determined as

$$\text{CEST}_{\text{asym}} = \frac{M_{\text{sat}}(-\Delta\omega) - M_{\text{sat}}(\Delta\omega)}{M_{\text{sat}}(-\Delta\omega)} \quad (6)$$

where M_{sat} refers to the magnetization with saturation at a positive ($\Delta\omega$) or a negative ($-\Delta\omega$) offset from the water resonance.¹³

The metabolites that were used for the multi-pool simulation of the human brain were Ala (0.3 mM), GABA (1.5 mM), Asp (2.2 mM), Gln (2.0 mM), Glu (11.0 mM) and Tau (2.0 mM).^{25,26} The simulations for the brain of polar cod were based on the following metabolite concentrations: Ala (1.0 mM), GABA (2.8 mM), Gln (2.5 mM), Glu (5.0 mM) and Tau (20 mM) ($t_{\text{Cr}} = 7 \text{ mM}$).²³

The relaxation times for water at 37°C as a function of B_0 were chosen as published by Khlebnikov *et al.*: $T_1/T_2 = 1.8 \text{ s}/55 \text{ ms}$ (at 7 T), $2.1 \text{ s}/42 \text{ ms}$ (at 9.4 T), $2.11 \text{ s}/37 \text{ ms}$ (at 11.7 T) and $2.45 \text{ s}/25.9 \text{ ms}$ (at 14.1 T).¹¹ For the simulation for the brain of the polar cod, T_1 and T_2 at 7 T were determined experimentally, and further the same B_0 dependence as described by Khlebnikov *et al.* was assumed.

3 | RESULTS

3.1 | Dependence of k_{sw} of amine protons on pH and temperature

Figure 1 depicts the experimentally determined exchange rates (circles) and the model functions $k_{sw}(pH, T)$ for the amino acids Ala, GABA, Asp, Gln, Glu and Tau. Note the different scaling for Gln and Tau. The quality for all fits was above $R^2 = 0.98$.

For all metabolites, the experimentally determined k_{sw} values show an exponential behavior as a function of pH and temperature. Using Equations 1-5 base- and buffer-catalyzed exchange rate constants and activation energies were obtained for the different amino acids, as shown in Table 1. Also, the pK values of the amine protons of the amino acids were included in Table 1 as a basis for the following discussion.⁴⁷ Note that the effective base-catalyzed rate constant for Tau is a factor of 10 higher compared with Ala, GABA, Asp and Glu, while their effective activation energy is the lowest.

3.2 | Dependence of the CEST effect on B_0 , B_1 amplitude and t_{sat}

Table 2 displays the experimental parameters B_1 and t_{sat} for the maximal CEST effect at 37 °C as found in measurements on humans or rodents. No reliable results could be determined for Gln and Tau because at a temperature of 37 °C their k_{sw} values are too high to be in the sensitive

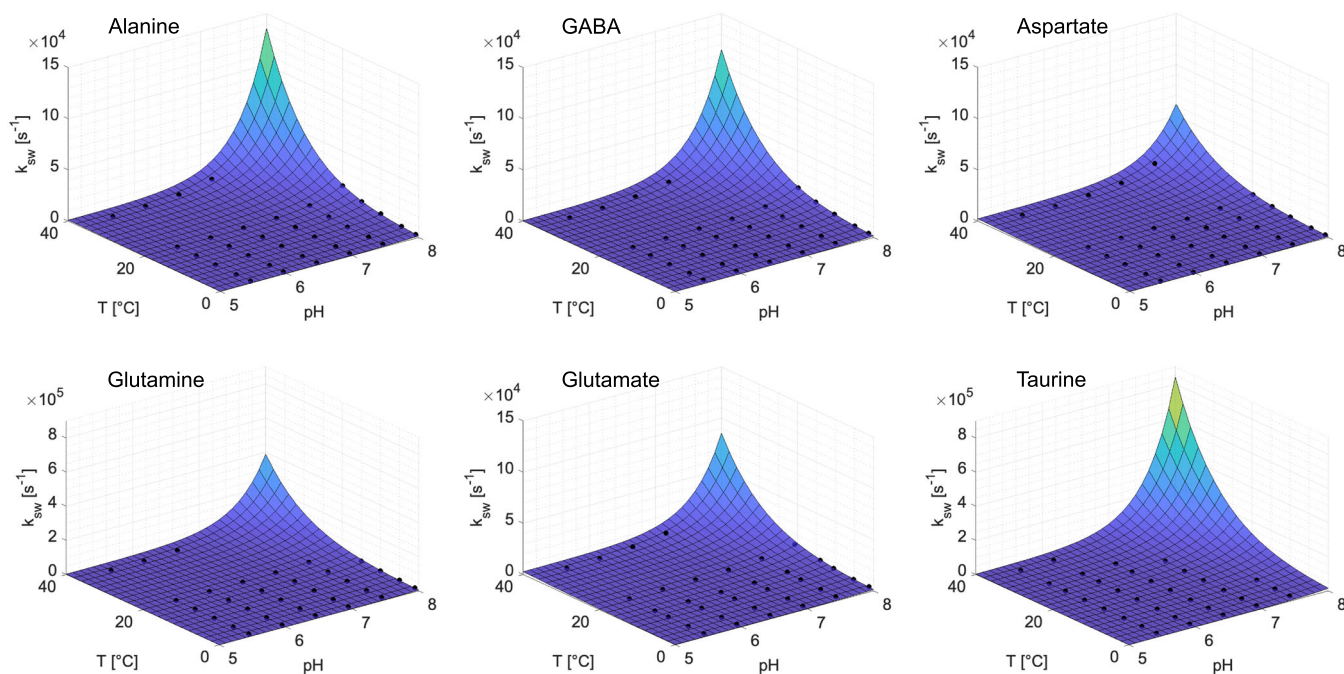


FIGURE 1 Experimentally determined exchange rates (k_{sw}) [s^{-1}] (circles) and fitted model functions $k_{sw}(pH, T)$ for the metabolites Ala, GABA, Asp, Gln, Glu and Tau (see Equations 1-4 and Table 1)

TABLE 1 Base- and buffer-catalyzed exchange rate constants and activation energies of different amino acids which can be used for Equation 5 (cf. Section 2)

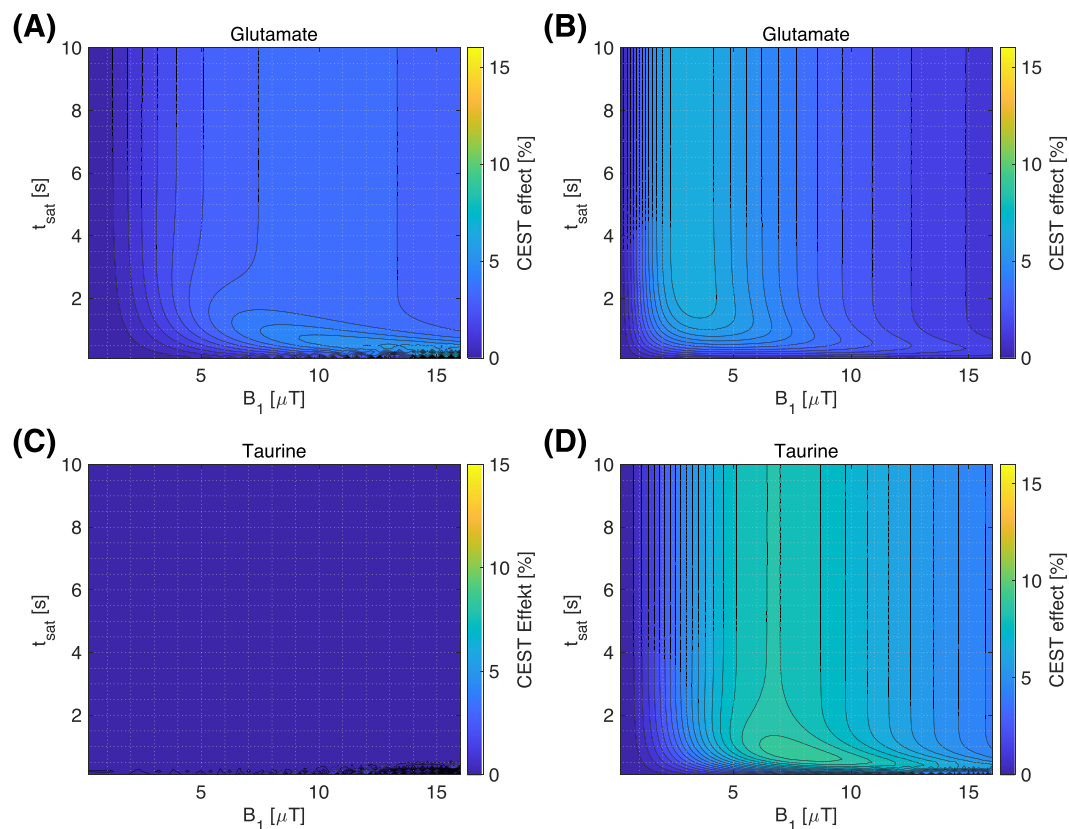
Metabolite	Effective base-catalyzed rate constant $k_{base, eff}(298.15\text{ K})$ [$s^{-1}\text{ L mol}^{-1}$]	Effective activation energy $E_{A, base, eff}$ [kJ mol^{-1}]	Effective buffer-catalyzed rate constant $k_{buffer, eff}(298.15\text{ K})$ [$s^{-1}\text{ L mol}^{-1}$]	Effective activation energy $E_{A, buffer, eff}$ [kJ mol^{-1}]	pK value ($-\text{NH}_2$ at $\approx 2.8\text{ ppm}$; $25\text{ }^\circ\text{C}$)
Ala	$(2.8 \pm 0.1) \times 10^{10}$	24.0 ± 1.8	522.1 ± 53.3	28.8 ± 4.4	9.87
GABA	$(2.6 \pm 0.1) \times 10^{10}$	20.7 ± 2.1	212.4 ± 16.9	31.4 ± 3.6	10.56
Asp	$(1.4 \pm 0.1) \times 10^{10}$	18.8 ± 3.8	976.5 ± 30.7	43.0 ± 1.3	9.90
Gln	$(8.6 \pm 1.6) \times 10^{10}$	22.1 ± 8.3	1111.7 ± 338.7	26.1 ± 13.5	9.13
Glu	$(1.9 \pm 0.2) \times 10^{10}$	20.5 ± 5.5	1169.4 ± 90.8	42.3 ± 3.4	9.47
Tau	$(2.1 \pm 0.1) \times 10^{11}$	15.8 ± 3.5	1147.8 ± 123.4	20.8 ± 4.2	9.06

TABLE 2 Experimental parameters yielding the largest CEST effects for Ala, Asp, GABA and Glu at different field strengths at 37 °C (pH 7.0, 10 mM), based on the measurements described above

Metabolites	B_1 [μ T]				Saturation time [s]			
	7 T	9.4 T	11.7 T	14.1 T	7 T	9.4 T	11.7 T	14.1 T
Ala (2.8 ppm)	11.2	15.6	16.0	16.0	0.6	0.4	0.5	0.5
Asp (2.8 ppm)	15.8	13.4	15.0	15.2	0.4	0.5	0.5	0.5
GABA (2.75 ppm)	15.2	15.8	15.8	15.6	0.4	0.4	0.5	0.5
Glu (3.0 ppm)	16.0	16.0	16.0	16.0	0.2	0.4	0.5	0.5

TABLE 3 Experimental parameters yielding the largest CEST effects for Ala, Asp, GABA, Gln, Glu and Tau at different field strengths at 1.5 °C (pH 7.0, 10 mM), based on the measurements described above

Metabolites	B_1 [μ T]				Saturation time [s]			
	7 T	9.4 T	11.7 T	14.1 T	7 T	9.4 T	11.7 T	14.1 T
Ala (2.8 ppm)	3.0	3.0	3.0	2.8	3.1	3.9	4.5	4.7
Asp (2.8 ppm)	2.8	2.8	2.8	2.6	3.5	4.4	5.0	5.3
GABA (2.75 ppm)	2.4	2.4	2.4	2.4	4.4	5.5	6.3	6.0
Gln (2.8 ppm)	4.8	5.0	5.0	4.8	1.5	1.8	2.0	2.1
Glu (3.0 ppm)	3.2	3.2	3.2	3.0	3.1	3.9	4.5	4.7
Tau (2.8 ppm)	7.6	8.0	8.2	8.0	0.8	0.9	1.0	1.0

**FIGURE 2** Simulated CEST effects as a function of B_1 and t_{sat} for Glu at 37 °C (A) and 1.5 °C (B) and for Tau at 37 °C (C) and 1.5 °C (D) (10 mM, pH 7, $B_0 = 7$ T)

ranges for CEST imaging. On average, for a maximum CEST effect at a body temperature of 37 °C, a higher B_0 requires a higher B_1 and a longer t_{sat} .

Table 3 summarizes the results for the experimental parameters that achieve the maximum CEST effect in the brain of the polar cod at 1.5 °C. In contrast to an application at 37 °C, on average, a lower B_1 with higher B_0 but longer t_{sat} is required to achieve the maximum CEST effect at 1.5 °C. Note that compared with the other amino acids significantly higher B_1 and shorter t_{sat} are required for Gln and Tau.

Figure 2 presents the different CEST effects and their optimal experimental parameters B_1 and t_{sat} at 37 °C and at 1.5 °C for the amino acids Glu (A, B) and Tau (C, D). While for Glu at 37 °C a high B_1 amplitude and relatively short t_{sat} would be optimal (Figure 2A), the maximum GluCEST effect at 1.5 °C can be achieved with a much lower B_1 amplitude and a longer t_{sat} (Figure 2B). For Tau, however, no significant CEST effect can be detected at 37 °C and pH 7 (Figure 2C), but this changes when the temperature becomes 1.5 °C, whereby a significant effect can be seen with a high B_1 amplitude and a short t_{sat} (Figure 2D).

Figure 3 shows the total *in vivo* expected CEST effect and the specificity of the dominating metabolite, i.e. its percentage contribution to the total CEST effect, as a function of the experimental parameters B_1 and t_{sat} . For the human brain, the total CEST effect (A) (7 T) and the specificity of the dominant metabolite Glu (C) are displayed, while the total CEST effect as expected *in vivo* in the brain of polar cod (B) (9.4 T) and the specificity of Tau (D) are shown.

The *in vivo* expected CEST effects for both organisms require a relatively large B_1 amplitude and a short t_{sat} for maximum signal intensity. For the simulation of the specificity of the GluCEST effect for the human brain, the contour plots clearly show that independent of the B_1 amplitude and t_{sat} the proportion of Glu in the total CEST effect is always between 68% and 71%. In contrast, the specificity of TauCEST in the fish model shows a strong dependence on the B_1 amplitude. However, the average percentage of Tau is above 50%, and it can be up to 78%.

3.3 | Intensity and specificity of the CEST effects of amino acids

Figure 4 illustrates the *in vivo* expected CEST effects with optimized experimental parameters for the human brain (A) ($B_1 = 3.6 \mu\text{T}$, 3.0 ppm, 7 T) and for the brain of polar cod (B) ($B_1 = 4.4 \mu\text{T}$, 2.8 ppm, 9.4 T) as a function of pH and temperature. Figure 4C and 4D shows the specificity for

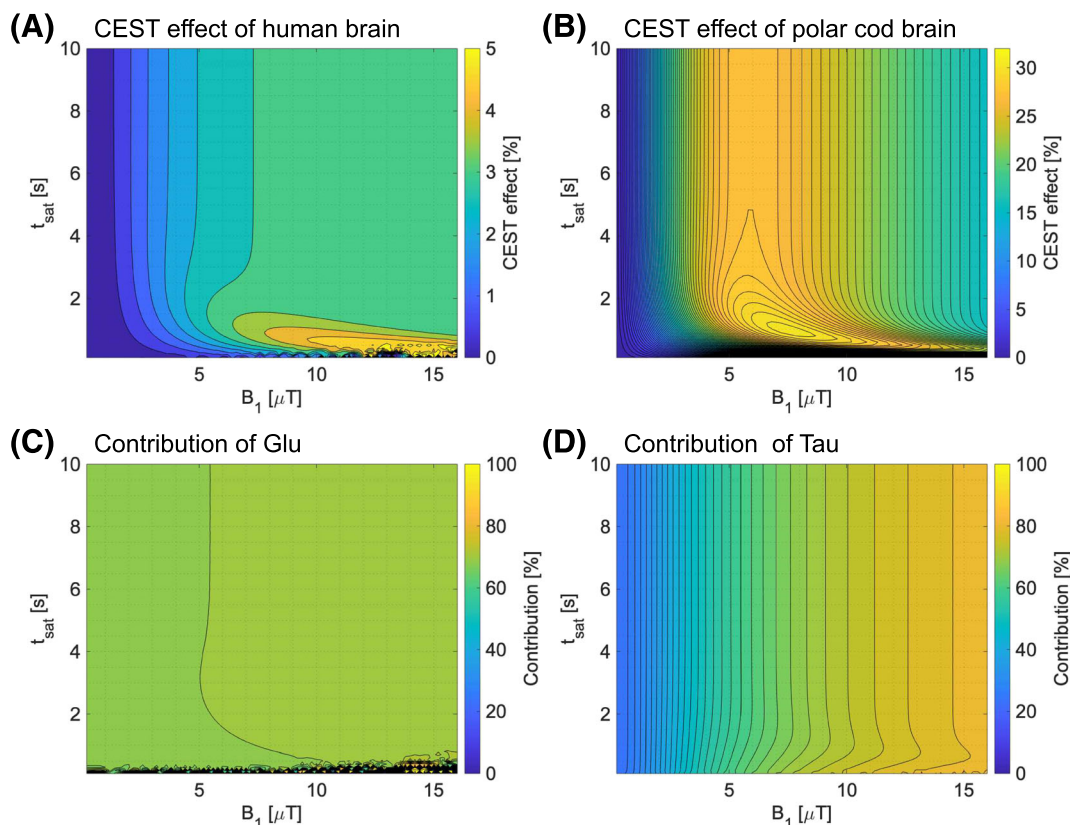


FIGURE 3 Simulated *in vivo* expected CEST effects and the contributions for the dominant metabolite as a function of B_1 and t_{sat} : total CEST effect for the human brain (37 °C) at 3 ppm (A) and the contribution of Glu (C) (7 T), and total CEST effect for the polar cod (1.5 °C) at 2.8 ppm (B) and the contribution of Tau (D) (9.4 T). The contour plots overlaid on the maps represent the regions with steps of 0.5% for the plots of the total CEST effects and 2% for the maps of the corresponding contributions of Glu and Tau

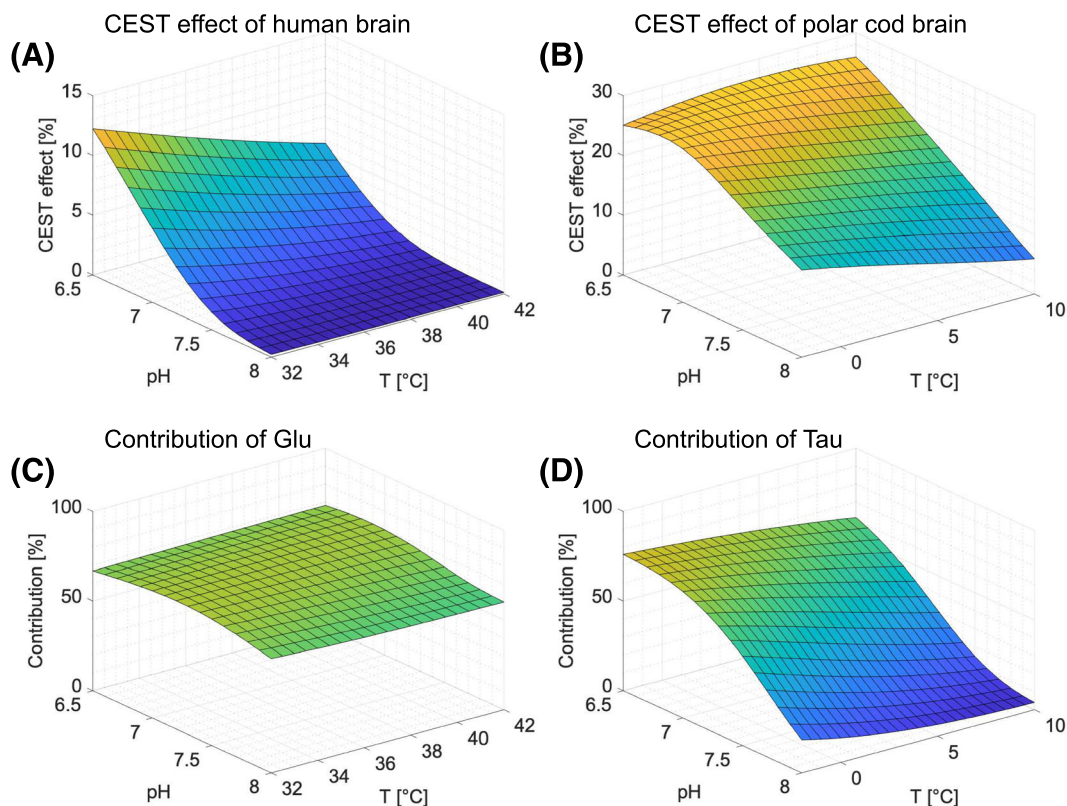


FIGURE 4 Simulated *in vivo* expected CEST effects and the contributions of the dominant metabolite as a function of pH and temperature: CEST effect for the human brain at 3 ppm (A) and the corresponding contribution of Glu (C) ($3.6 \mu\text{T}$, 7 T, 37°C), and CEST effect for the polar cod at 2.8 ppm (B) and the contributions of its major metabolite Tau (D) ($4.4 \mu\text{T}$, 9.4 T, 1.5°C)

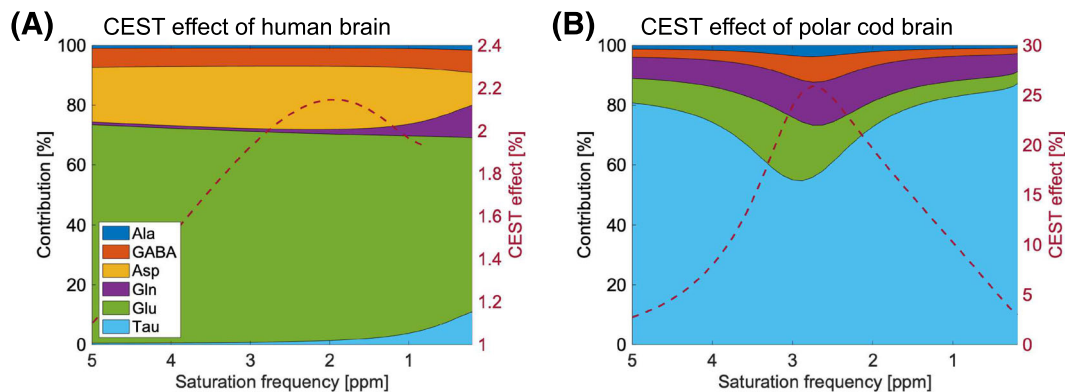


FIGURE 5 Simulations of the expected contributions of the metabolites to the *in vivo* expected CEST effects (red dotted line) as a function of the saturation frequency for the human brain (pH 7.2, 37°C , $3.6 \mu\text{T}$, 7 T) (A) and for the brain of polar cod (pH 7.2, 1.5°C , $4.4 \mu\text{T}$, 9.4 T) (B)

Glu (human brain) and Tau (polar cod brain). For the two simulations, an increase of the total CEST effect with decreasing pH value occurs. While in the human brain a rise in temperature results in a lower CEST effect, the same is true for the effect in the brain of the polar cod for basic pH values, but it turns into an increase in the effect for the more acidic pH range. The specificity for GluCEST in the human brain shows almost no change depending on pH and temperature and is approximately constant at 70%. The dependence of the specificity of the TauCEST effect in the brain of polar cod is different, with a strong increase in the acidic pH range and for lower temperature.

The contributions of the different amino acids to the *in vivo* expected CEST effect in the human brain and the brain of polar cod as a function of the saturation frequency are shown in Figure 5. The main percentage contribution of Glu to the total CEST effect in the human brain is almost independent of the saturation frequency, while the remaining percentage is mainly due to Asp and GABA (see Figure 5A). Although for all saturation frequencies the main contribution to the CEST effect in the brain of polar cod is due to Tau, it is noteworthy that its percentage contribution is lowest at the maximum intensity of the total CEST effect (see Figure 5B). The remaining contributions are mainly due to Glu and Gln.

4 | DISCUSSION

This work aimed to characterize the amine proton exchange of important amino acids. Therefore, the exchange rates of six amino acids were determined experimentally as a function of pH and temperature and the influence of experimental parameters was simulated. The intensity and specificity of the CEST effect of amino acids at about 2.8 ppm as expected in the human brain were analyzed by simulations. Furthermore, this was also done for an ectothermic animal model, the polar cod, to demonstrate the strong temperature dependence and the broad applicability of the CEST effect.

4.1 | Dependence of k_{sw} of amine protons on pH and temperature

The CEST effect at about 2.8 ppm is, besides other things, largely determined by exchangeable amine protons of relatively highly concentrated amino acids, in particular Ala, GABA, Asp, Gln, Glu and Tau. Other important metabolites involved in brain metabolism, such as glucose (-OH, 1.2 ppm),⁴⁸ creatine ($-\text{NH}_2$)₂⁺, 1.9 ppm)⁴⁹ and myo-inositol (-OH, 0.6 ppm),⁵⁰ can be neglected in this consideration, as their effects are almost not involved in the total CEST effect at about 2.8 ppm for a physiological pH of 7.2.

The exchange rates were determined by numerical fitting of the Bloch-McConnell equation. Two approaches to determine the exchange rates of exchangeable protons based on the CEST effect have been published by McMahon *et al.*⁵¹ These quantification methods use the fact that the exchange is a function of both the t_{sat} (QUEST; quantifying exchange using saturation time) and the B_1 amplitude of saturation (QUESP; quantifying exchange using saturation power). However, the validity of these approaches is limited to rather slow exchange rates that fulfill the conditions $k_{sw} \ll \omega_1$ (nutating rate of the RF irradiation) and $k_{sw} \ll \Delta\omega$, as they apply to the amide protons of, e.g., poly-L-lysine (PLL), but not to the amine protons investigated here, which are characterized by faster exchange rates.¹¹ Randtke *et al.* were able to describe the so-called HW-QUESP method, based on the Hanes-Woolf diagram, as an evaluation method for enzyme kinetics.³⁹ This method is a suitable approach for the determination of fast exchange rates, but the numerical fits of the Bloch-McConnell equation provide more precise results. Spectroscopic methods for determining exchange rates, such as WEX spectroscopy (water-exchange filter spectroscopy),^{52,53} are limited to very slow exchange processes.⁵¹ Potential errors in the fit of z-spectra with the Bloch-McConnell equation may arise from other than the proton group of interest. In our study, only Gln has another group of labile bound protons at 2.2 ppm, which is characterized by a very slow exchange rate of less than 50 s^{-1} , that, following the Arrhenius equation (see Equation (2)), slows down further with decreasing temperatures; therefore, at a B_1 amplitude of 5.87 μT such slow exchanging protons can be neglected.

Due to the dominant base catalysis (see Equation (3)) and the Arrhenius equation (see Equation (2)), the exchange rates experimentally determined for the different metabolites show the expected mono-exponential course as a function of pH and temperature. Lee *et al.* assigned the resonances of exchangeable protons of brain metabolites and the positions and full widths at half maximum of the signals using ¹H NMR spectra measured on a high-resolution 11.7 T spectrometer.¹⁰ The exchange rates determined on this basis are in some cases lower than the values found in the present study. One reason for this is that the method used by Lee *et al.* to determine exchange rates using the half-width is limited in its validity to slow exchange regimes.⁵¹ Furthermore, the solutions were prepared without the use of a corresponding phosphate buffer. However, amine and hydroxyl protons of amino acids show a strong dependence on buffer properties, as they occur in the natural environment.⁵⁴ The osmolarity and concentration of phosphate, therefore, has a catalytic effect for the exchange of the amine protons and must be included in the considerations for an analysis of the *in vivo* CEST effect expected at about 2.8 ppm. Khlebnikov *et al.* measured the k_{sw} for the most important metabolites for the CEST effect in the human brain in the physiological pH range at 37 °C.¹¹ Although the exchange rates in both these and the present work were determined by fitting z-spectra with the Bloch-McConnell equation, the exchange rates determined by Khlebnikov *et al.* are slightly but systematically lower. This difference may be attributed to the 2 mM higher concentrated PBS solution used in the present study and its influence on the exchange rates as described above.

The acid constants (pK value) of the amino groups of the metabolites investigated vary within a range of 9.0-10.6 units (see Table 1). According to the Brønsted law of acid/base catalysis, the logarithm of k_{sw} is proportional to the pK value of the amine protons,^{55,56} which is reflected in the data obtained. A comparison of the pK values and the determined exchange rates for 25 °C and pH 7.0 shows a similar order, i.e. a lower pK value corresponds to a faster k_{sw} . In addition, the exchange rates of Glu and Asp show a comparable behavior due to similar pK values.¹⁰ Furthermore, the remarkably fast exchange rates of Gln and Tau match their low pK values.

A determination of $k_{sw}(\text{pH}, T)$ supports both the analysis of CEST effects and the optimization of the pulse sequences used.¹⁴ For this reason, the experimentally determined exchange rates were interpolated based on the Equations 1-5 and the base- and buffer-catalyzed exchange rates and activation energies for the different metabolites were determined (see Figure 1 and Table 1).

The determined effective base-catalyzed exchange rates ($k_{b,\text{eff}}$) for amine protons ($T = 25 \text{ °C}$) are higher by a power of 10 than those for the base-catalyzed exchange of amide protons of PLL $k_b(37 \text{ °C}) = 1.92 \times 10^9 \text{ s}^{-1} \text{ L mol}^{-1}$ ⁵¹ and of guanidinium protons of creatine $k_{b,\text{eff}}(25 \text{ °C}) = (3.01 \pm 0.16) \times 10^9 \text{ s}^{-1} \text{ L mol}^{-1}$.¹⁴ The base-catalyzed exchange rates for the amine protons of GABA, Gln, Glu and Tau in the work of Khlebnikov *et al.* are in the same order of magnitude as those determined in the present work.¹¹ Differences can be explained by the slight deviations in the

determination of the exchange rates described above and by the different temperatures on which the analysis is based. The base-catalyzed exchange constants are an indicator of the sensitivity of the exchange rates as a function of the pH value. Thus, pH changes have a much greater influence on the exchange of Tau and Gln than that, for example, of Asp.

The activation energies of the base-catalyzed exchange, $20.32 \text{ kJ mol}^{-1}$ on average, are lower than those determined for amide protons of peptide groups ($71.12 \text{ kJ mol}^{-1}$)⁴⁴ and the guanidinium protons of creatine ($32.27 \text{ kJ mol}^{-1}$).¹⁴ This aspect fits the high exchange rates of the amine protons compared to the amide and guanidinium protons, since the lower the activation energy the faster the reaction proceeds. Liepinsh and Otting were able to show that amino acids whose amino groups have a low pK value are more sensitive to buffer properties than those with higher pK values.⁵⁴ This is reflected in the data obtained for buffer-catalyzed exchange rates (see Table 1).

4.2 | Dependence of the CEST effect on B_0 , B_1 amplitude and t_{sat}

On the basis of the experimentally determined model functions $k_{\text{sw}}(\text{pH}, T)$ for the different amino acids, the influence of the experimental parameters B_0 , B_1 and t_{sat} was investigated at two different temperatures (10 mM, 1.5°C and 37°C) (see Tables 2,3 and Supplementary Material). These findings can be used as a starting point for the optimization of existing pulse sequences, but also as a basis for the development of new CEST sequences and processing models.

As reflected in our results the intensity of the CEST effect increases with higher B_0 (see Supplementary Material), since $\Delta\omega$ increases proportionally to the magnetic field strength and thus the influence of direct saturation of water is reduced. As a result, even metabolites with faster exchange rates meet the requirements for the CEST effect, i.e. a slow to medium exchange regime $k_{\text{sw}} \leq \Delta\omega$. Also, the T_1 relaxation time increases with a higher B_0 field, which delays the time until thermodynamic equilibrium is reached and can lead to a higher CEST effect. Additionally, the CEST effect increases with B_1 but decreases again when direct saturation becomes important (see also Figures 2 and 3).⁵⁷ When a very high B_1 amplitude is selected, the CEST effect is partially or even completely cancelled out (see Figures 2 and 3).^{35,57} The influence of the B_1 amplitude on the CEST effect can be explained most simply in terms of the saturation efficiency α . This parameter, introduced by Sun *et al.*, is a measure of the intensity of the maximum CEST effect and depends on both k_{sw} and the applied B_1 amplitude.⁵⁸ In general, a faster k_{sw} requires a higher B_1 amplitude to achieve the same CEST effect and similar saturation efficiency (see Figure 2). The CEST effect builds up over a defined t_{sat} , whereby after a defined saturation period of about $5 T_{1w}$ the thermodynamic equilibrium state is reached. However, the influence of the direct saturation shows a biexponential behavior as a function of t_{sat} , and since interferences with direct water saturation increase with t_{sat} , an optimal t_{sat} can exist for faster-exchanging systems where the spillover is not yet fully effective (see Figure 2).⁵⁷

The temperature dependence of exchange rates is characterized by the Arrhenius equation.⁴⁴ Accordingly, even small temperature changes can have a large effect on the exchange rate, given the exponential relationship. As a consequence, metabolites with a fast exchange at high temperatures can be assigned to the slow to medium exchange regime at lower temperatures and become of interest for CEST imaging (e.g. Tau). Due to the relationships between the experimental parameters and the exchange rate discussed in the previous section, a temperature change thus also results in different optimal experimental parameters for CEST imaging (see Figure 2). This aspect is still strongly influenced by different composition of metabolite concentrations in different organisms or at different (patho-) physiological conditions (see Figure 3).

At present, CEST measured *in vivo* is often described as a metabolite weighted contrast emphasizing the main contribution of one metabolite.¹¹ However, it is important to consider the contributions of other compounds and the dependence of the specificity on temperature and pH to avoid physiological misinterpretations. In a recent study by Chen *et al.*, the authors conclude that tCr accounts for 80% of the guanidinium peak of the CEST effect in the brain of a mouse at optimal experimental parameters. Cai *et al.* showed that the CEST effect observed *in vivo* in the human brain is mainly determined by Glu, with a contribution of 70-75% (3 ppm, 37°C , 7 T).⁴ This result is well reflected in our simulations, where Glu dominates the *in vivo* expected CEST effect in the human brain independent of the experimental parameters, with a share of 68-71%. The situation is different for the CEST effect expected *in vivo* for a model organism such as the polar cod, where the specificity of the Tau dominated *in vivo* CEST effect increases with increasing B_1 amplitude. An optimal choice of experimental parameters and a consistent analysis of the CEST effect as a multi-pool model together with adequate knowledge of the metabolite composition is therefore essential.

4.3 | Intensity and specificity of the CEST effects of amino acids

The choice of optimal experimental parameters is a trade-off between the intensity of the CEST effect and its specificity (see Figure 3). Additionally, the choice of saturation parameters is constrained by the specific absorption rate (SAR). As SAR increases with B_1 and B_0 , the allowed B_1 amplitude at 7 T is limited for human application.⁴ For this reason, a B_1 amplitude of $3.6 \mu\text{T}$, as already used by Cai *et al.*, was chosen for the simulations in the present study.⁴ These guidelines do not apply to *in vivo* applications on animal models such as polar cod. However, any uncontrolled body temperature due e.g. to heating of the surrounding seawater during the measurement should be avoided at all costs, so in the present work a B_1 of $4.4 \mu\text{T}$ at 9.4 T was used. This is consistent with previous *in vivo* applications, where no warming could be detected during the

temperature-controlled measurements.²² However, an optimization of the saturation scheme and RF pulse shapes can lead to an increase in the intensity of the CEST effect.

The simulations for the CEST effect for the human brain and the brain of the polar cod show considerable differences due to different metabolite concentrations and especially due to the different temperatures and thus different k_{sw} values (see Figure 4). The specificity of the metabolite dominating the CEST effect in the brain of polar cod at 1.5 °C is strongly dependent on pH and T. For high temperature and an acidic pH the k_{sw} of Glu is in the optimal slow- to intermediate-exchange regime ($k_{sw} \leq \Delta\omega$), whereas this optimal regime is reached for Tau at low temperature and basic pH.

Considerations of the *in vivo* expected CEST effect of amino acids for the human brain for various typical pathological conditions show that, e.g., for acute cerebral ischemia with acidification of pH by 0.3 pH units, an increase in the CEST effect can be expected, but the specificity of Glu remains at 70%. For the clinical picture of a glioblastoma, an alkalization of 0.5 pH units can be expected, but even in this particular case a slight decrease in specificity to 63% can be assumed.

The specificity of Tau behaves differently in the example of the brain of a polar cod. Polar cod can be easily exposed to temperature changes of 4 °C to −2 °C within a very short time due to, e.g., vertical movements in the water column; simulating this in an *in vivo* application would result in a change of the specificity of Tau of almost 20%, which in turn would result in a specificity below 50% for Tau. In contrast, acidification of pH_i due to acute incubation of polar cod with CO₂ to simulate ocean acidification scenarios (−0.2 pH units) would result in a 10% increase.

In a previous *in vivo* study on polar cod (see Supplementary Material), we could show that a simulated ocean acidification scenario (i.e. CO₂-enriched sea water (4900 μatm)) resulted in an increase by 3.2% of the CEST effect in brain of polar cod.²² According to our simulations, this corresponds to a decrease in pH_i by 0.4 pH units, as expected from the effect of elevated CO₂ concentrations in the blood.

These examples show that careful considerations of the specificity of the CEST effect are needed to minimize the risk of misinterpretations for different pH and temperature dependences of metabolites involved in the CEST effect. One approach can be the shift of the saturation frequency at which the analysis is performed (Figure 5). In contrast to the Glu weighted CEST effect in the human brain, whose specificity is nearly constant over the saturation frequencies studied, the specificity of Tau in the expected CEST effect in the brain of polar cod shows a strong dependence on the saturation frequency. An evaluation of the CEST effect at about 2 ppm would thus result in an approximately 20% increase in specificity. This is facilitated by a shift of the asymmetry curve for Tau towards lower ppm values due to intermediate- to fast-exchange chemical shift averaging.⁴ The rather small intensity loss of the CEST effect at this offset frequency can be neglected or compensated by extending the measurement time, i.e. averaging. The gain in specificity from the significantly reduced influence of other compounds on the total CEST effect, however, is much more desirable to avoid physiological misinterpretation.

The *in vivo* expected CEST effects presented in this study focus on the CEST effect of highly concentrated amino acids with exchangeable protons at about 2.8 ppm downfield from water and its behavior in terms of intensity and specificity for different experimental and physiological parameters. We have shown this for two very different organisms to demonstrate the wide range of CEST applications. However, it should be emphasized that other effects have been neglected in this study, such as MTC and upfield nuclear Overhauser enhancement, as there are several approaches to remove these effects from the *in vivo* CEST data, as mentioned in the introduction. Furthermore, the APT effect of amide protons of mobile proteins and peptides was not included in the modeling of this study. Amide protons are by far the most highly concentrated group of exchanging protons of mobile proteins, even if other groups occur at much lower concentrations. Furthermore, protein conformational changes, which can occur *in vivo*, further complicate their inclusion in simulations.¹¹

5 | CONCLUSION

In the present work, the exchange rates k_{sw} (pH, T) have been determined for six amino acids that are important for brain metabolism. These functions can be used for the simulation of multi-pool models of a wide variety of organisms and their physiological properties. Based on these multi-pool models, it is possible to optimize saturation parameters and improve the analysis of CEST effects of amino acids measured *in vivo*.

DATA AVAILABILITY STATEMENT

The data that support the findings of this study are available from the corresponding author upon reasonable request.

Data will be made available in a public repository after approval.

ORCID

Christian Bock  <https://orcid.org/0000-0003-0052-3090>

REFERENCES

1. Ward KM, Aletras AH, Balaban RS. A new class of contrast agents for MRI based on proton chemical exchange dependent saturation transfer (CEST). *J Magn Reson.* 2000;143(1):79-87. <https://doi.org/10.1006/jmre.1999.1956>

2. Neal A, Moffat BA, Stein JM, et al. Glutamate weighted imaging contrast in gliomas with 7 Tesla magnetic resonance imaging. *Neuroimage Clin.* 2019; 22:101694. <https://doi.org/10.1016/j.nicl.2019.101694>
3. Somkina NV, Krichevskaya AA. Amino acids in the fish brain. *Neurosci Behav Physiol.* 1969;3(1):14-18. <https://doi.org/10.1007/BF01125907>
4. Cai K, Haris M, Singh A, et al. Magnetic resonance imaging of glutamate. *Nat Med.* 2012;18(2):302-306. <https://doi.org/10.1038/nm.2615>
5. Haris M, Nath K, Cai K, et al. Imaging of glutamate neurotransmitter alterations in Alzheimer's disease. *NMR Biomed.* 2013;26(4):386-391. <https://doi.org/10.1002/nbm.2875>
6. Kogan F, Singh A, Debrosse C, et al. Imaging of glutamate in the spinal cord using GluCEST. *NeuroImage.* 2013;77:262-267. <https://doi.org/10.1016/j.neuroimage.2013.03.072>
7. Cai K, Singh A, Roalf DR, et al. Mapping glutamate in subcortical brain structures using high-resolution GluCEST MRI. *NMR Biomed.* 2013;26(10):1278-1284. <https://doi.org/10.1002/nbm.2949>
8. Singh A, Cai K, Haris M, Hariharan H, Reddy R. On B₁ inhomogeneity correction of *in vivo* human brain glutamate chemical exchange saturation transfer contrast at 7T. *Magn Reson Med.* 2013;69(3):818-824. <https://doi.org/10.1002/mrm.24290>
9. Haris M, Singh A, Cai K, et al. High resolution mapping of modafinil induced changes in glutamate level in rat brain. *PLoS ONE.* 2014;9(7):e103154. <https://doi.org/10.1371/journal.pone.0103154>
10. Lee J-S, Xia D, Jerschow A, Regatte RR. *In vitro* study of endogenous CEST agents at 3 T and 7 T. *Contrast Media Mol Imaging.* 2016;11(1):4-14. <https://doi.org/10.1002/cmml.1652>
11. Khlebnikov V, van der Kemp WJM, Hoogduin H, Klomp DWJ, Prompers JJ. Analysis of chemical exchange saturation transfer contributions from brain metabolites to the Z-spectra at various field strengths and pH. *Sci Rep.* 2019;9(1):1089. <https://doi.org/10.1038/s41598-018-37295-y>
12. Cai K, Haris M & Singh A et al. Magnetic Resonance imaging of the neurotransmitter GABA *in vivo*. In Proceedings of the Joint Annual Meeting ISMRM-ESMRMB, Stockholm, Sweden. 2010:2983.
13. Wermter FC, Bock C, Dreher W. Investigating GluCEST and its specificity for pH mapping at low temperatures. *NMR Biomed.* 2015;28(11):1507-1517. <https://doi.org/10.1002/nbm.3416>
14. Goerke S, Zaiss M, Bachert P. Characterization of creatine guanidinium proton exchange by water-exchange (WEX) spectroscopy for absolute-pH CEST imaging *in vitro*. *NMR Biomed.* 2014;27(5):507-518. <https://doi.org/10.1002/nbm.3086>
15. Van der Linden A, Van Meir V, Tindemans I, Verhoye M, Balthazart J. Applications of manganese-enhanced magnetic resonance imaging (MEMRI) to image brain plasticity in song birds. *NMR Biomed.* 2004;17(8):602-612. <https://doi.org/10.1002/nbm.936>
16. Van der Linden A, Verhoye M, Pörtlner HO, Bock C. The strengths of *in vivo* magnetic resonance imaging (MRI) to study environmental adaptational physiology in fish. *Magn Reson Mater Phys Biol Med.* 2004;17(3-6):236-248. <https://doi.org/10.1007/s10334-004-0078-0>
17. Kabli S, Spaink HP, De Groot HJM, Alia A. *In vivo* metabolite profile of adult zebrafish brain obtained by high-resolution localized magnetic resonance spectroscopy. *J Magn Reson Imaging.* 2009;29(2):275-281. <https://doi.org/10.1002/jmri.21609>
18. Kabli S, He S, Spaink HP, et al. *In vivo* magnetic resonance imaging to detect malignant melanoma in adult zebrafish. *Zebrafish.* 2010;7(2):143-148. <https://doi.org/10.1089/zeb.2009.0649>
19. Merrifield GD, Mullin J, Gallagher L, et al. Developing cardiac magnetic resonance imaging in the live zebrafish. *Heart.* 2015;101(Suppl 6):A6. <https://doi.org/10.1136/heartjnl-2015-308734.16>
20. Merrifield G, Mullin J, Gallagher L, et al. *In vivo* cardiac magnetic resonance imaging of adult zebrafish. *Heart.* 2015;101(Suppl 4):A96-A97. <https://doi.org/10.1136/heartjnl-2015-308066.170>
21. Koth J, Maguire ML, McClymont D, et al. High-resolution magnetic resonance imaging of the regenerating adult zebrafish heart. *Sci Rep.* 2017;7(1):2917. <https://doi.org/10.1038/s41598-017-03050-y>
22. Wermter FC, Maus B, Pörtlner HO, Dreher W, Bock C. CO₂ induced pH_i changes in the brain of polar fish: a TauCEST application. *NMR Biomed.* 2018; 31(8):e3955. <https://doi.org/10.1002/nbm.3955>
23. Schmidt M, Windisch HS, Ludwichowski KU, et al. Differences in neurochemical profiles of two gadid species under ocean warming and acidification. *Front Zool.* 2017;14(1):49. <https://doi.org/10.1186/s12983-017-0238-5>
24. Boyd TA, Cha CJ, Forster RP, Goldstein L. Free amino acids in tissues of the skate *Raja erinacea* and the stingray *Dasyatis sabina*: effects of environmental dilution. *J Exp Zool.* 1977;199(3):435-442. <https://doi.org/10.1002/jez.1401990318>
25. Pfeuffer J, Tkáč I, Provencher SW, Gruetter R. Toward an *in vivo* neurochemical profile: quantification of 18 metabolites in short-echo-time ¹H NMR spectra of the rat brain. *J Magn Reson.* 1999;141(1):104-120. <https://doi.org/10.1006/jmre.1999.1895>
26. Mlynárik V, Cudalbu C, Xin L, Gruetter R. ¹H NMR spectroscopy of rat brain *in vivo* at 14.1 Tesla: improvements in quantification of the neurochemical profile. *J Magn Reson.* 2008;194(2):163-168. <https://doi.org/10.1016/j.jmr.2008.06.019>
27. Tkáč I, Oz G, Adriany G, Uğurbil K, Gruetter R. *In vivo* ¹H NMR spectroscopy of the human brain at high magnetic fields: metabolite quantification at 4T vs. 7T. *Magn Reson Med.* 2009;62(4):868-879. <https://doi.org/10.1002/mrm.22086>
28. Hong ST, Balla DZ, Shajan G, Choi C, Uğurbil K, Pohmann R. Enhanced neurochemical profile of the rat brain using *in vivo* ¹H NMR spectroscopy at 16.4 T. *Magn Reson Med.* 2011;65(1):28-34. <https://doi.org/10.1002/mrm.22609>
29. Kiyatkin EA, Brown PL. Brain and body temperature homeostasis during sodium pentobarbital anesthesia with and without body warming in rats. *Physiol Behav.* 2005;84(4):563-570. <https://doi.org/10.1016/j.physbeh.2005.02.002>
30. Zhou J, Lal B, Wilson DA, Lartera J, van Zijl PCM. Amide proton transfer (APT) contrast for imaging of brain tumors. *Magn Reson Med.* 2003;50(6):1120-1126. <https://doi.org/10.1002/mrm.10651>
31. Jones CK, Schlosser MJ, van Zijl PCM, Pomper MG, Golay X, Zhou J. Amide proton transfer imaging of human brain tumors at 3T. *Magn Reson Med.* 2006;56(3):585-592. <https://doi.org/10.1002/mrm.20989>
32. Jones CK, Polders D, Hua J, et al. *In vivo* three-dimensional whole-brain pulsed steady-state chemical exchange saturation transfer at 7 T. *Magn Reson Med.* 2012;67(6):1579-1589. <https://doi.org/10.1002/mrm.23141>
33. Gruetter R. Automatic, localized *in vivo* adjustment of all first- and second-order shim coils. *Magn Reson Med.* 1993;29(6):804-811. <https://doi.org/10.1002/mrm.1910290613>
34. Sun PZ, Farrar CT, Sorensen AG. Correction for artifacts induced by B₀ and B₁ field inhomogeneities in pH-sensitive chemical exchange saturation transfer (CEST) imaging. *Magn Reson Med.* 2007;58(6):1207-1215. <https://doi.org/10.1002/mrm.21398>

35. Zaiss M, Schmitt B, Bachert P. Quantitative separation of CEST effect from magnetization transfer and spillover effects by Lorentzian-line-fit analysis of z-spectra. *J Magn Reson*. 2011;211(2):149-155. <https://doi.org/10.1016/j.jmr.2011.05.001>
36. Woessner DE, Zhang S, Merritt ME, Sherry AD. Numerical solution of the Bloch equations provides insights into the optimum design of PARACEST agents for MRI. *Magn Reson Med*. 2005;53(4):790-799. <https://doi.org/10.1002/mrm.20408>
37. Sun PZ. Simplified and scalable numerical solution for describing multi-pool chemical exchange saturation transfer (CEST) MRI contrast. *J Magn Reson*. 2010;205(2):235-241. <https://doi.org/10.1016/j.jmr.2010.05.004>
38. Nelder JA, Mead R. A simplex method for function minimization. *Comput J*. 1965;7(4):308-313. <https://doi.org/10.1093/comjnl/7.4.308>
39. Randtke EA, Chen LQ, Corrales LR, Pagel MD. The Hanes-Woolf linear QUESP method improves the measurements of fast chemical exchange rates with CEST MRI. *Magn Reson Med*. 2014;71(4):1603-1612. <https://doi.org/10.1002/mrm.24792>
40. Zong X, Wang P, Kim SG, Jin T. Sensitivity and source of amine-proton exchange and amide-proton transfer magnetic resonance imaging in cerebral ischemia. *Magn Reson Med*. 2014;71(1):118-132. <https://doi.org/10.1002/mrm.24639>
41. Jin T, Autio J, Obata T, Kim SG. Spin-locking versus chemical exchange saturation transfer MRI for investigating chemical exchange process between water and labile metabolite protons. *Magn Reson Med*. 2011;65(5):1448-1460. <https://doi.org/10.1002/mrm.22721>
42. Woodward CK, Hilton BD. Hydrogen isotope exchange kinetics of single protons in bovine pancreatic trypsin inhibitor. *Biophys J*. 1980;32(1):561-575. [https://doi.org/10.1016/S0006-3495\(80\)84990-3](https://doi.org/10.1016/S0006-3495(80)84990-3)
43. Eriksson MA, Härd T, Nilsson L. On the pH dependence of amide proton exchange rates in proteins. *Biophys J*. 1995;69(2):329-339. [https://doi.org/10.1016/S0006-3495\(95\)79905-2](https://doi.org/10.1016/S0006-3495(95)79905-2)
44. Bai Y, Milne JS, Mayne L, Englander SW. Primary structure effects on peptide group hydrogen exchange. *Proteins*. 1993;17(1):75-86. <https://doi.org/10.1002/prot.340170110>
45. Zhou J, Payen JF, Wilson DA, Traystman RJ, van Zijl PCM. Using the amide proton signals of intracellular proteins and peptides to detect pH effects in MRI. *Nat Med*. 2003;9(8):1085-1090. <https://doi.org/10.1038/nm907>
46. Sun PZ, Benner T, Kumar A, Sorensen AG. Investigation of optimizing and translating pH-sensitive pulsed-chemical exchange saturation transfer (CEST) imaging to a 3T clinical scanner. *Magn Reson Med*. 2008;60(4):834-841. <https://doi.org/10.1002/mrm.21714>
47. Dawson RMC, Elliot DC, Elliot WH, Jones KM. *Data for Biochemical Research*. 3rd ed. USA: Oxford University Press; 1989.
48. Chan KWY, McMahon MT, Kato Y, et al. Natural D-glucose as a biodegradable MRI contrast agent for detecting cancer. *Magn Reson Med*. 2012;68(6):1764-1773. <https://doi.org/10.1002/mrm.24520>
49. Haris M, Nanga RPR, Singh A, et al. Exchange rates of creatine kinase metabolites: feasibility of imaging creatine by chemical exchange saturation transfer MRI. *NMR Biomed*. 2012;25(11):1305-1309. <https://doi.org/10.1002/nbm.2792>
50. Haris M, Cai K, Singh A, Hariharan H, Reddy R. *In vivo* mapping of brain myo-inositol. *Neuroimage*. 2011;54(3):2079-2085. <https://doi.org/10.1016/j.neuroimage.2010.10.017>
51. McMahon MT, Gilad AA, Zhou J, Sun PZ, Bulte JW, van Zijl PCM. Quantifying exchange rates in chemical exchange saturation transfer agents using the saturation time and saturation power dependencies of the magnetization transfer effect on the magnetic resonance imaging signal (QUEST and QUESP): pH calibration for poly-L-lysine and a starburst dendrimer. *Magn Reson Med*. 2006;55(4):836-847. <https://doi.org/10.1002/mrm.20818>
52. Mori S, Johnson MO, Berg JM, van Zijl PCM. Water exchange filter (WEX Filter) for nuclear magnetic resonance studies of macromolecules. *J Am Chem Soc*. 1994;116(26):11982-11984. <https://doi.org/10.1021/ja00105a044>
53. Mori S, Abeygunawardana C, Berg JM, van Zijl PCM. NMR study of rapidly exchanging backbone amide protons in staphylococcal nuclease and the correlation with structural and dynamic properties. *J Am Chem Soc*. 1997;119(29):6844-6852. <https://doi.org/10.1021/ja963351f>
54. Liepinsh E, Otting G. Proton exchange rates from amino acid side chains—implications for image contrast. *Magn Reson Med*. 1996;35(1):30-42. <https://doi.org/10.1002/mrm.1910350106>
55. Brønsted JN. Acid and basic catalysis. *Chem Rev*. 1928;5(3):231-338. <https://doi.org/10.1021/cr60019a001>
56. Desmond KL, Stanisz GJ. Understanding quantitative pulsed CEST in the presence of MT. *Magn Reson Med*. 2012;67(4):979-990. <https://doi.org/10.1002/mrm.23074>
57. Zaiss M, Bachert P. Chemical exchange saturation transfer (CEST) and MR Z-spectroscopy *in vivo*: a review of theoretical approaches and methods. *Phys Med Biol*. 2013;58(22):R221-R269. <https://doi.org/10.1088/0031-9155/58/22/R221>
58. Sun PZ, van Zijl PCM, Zhou J. Optimization of the irradiation power in chemical exchange dependent saturation transfer experiments. *J Magn Reson*. 2005;175(2):193-200. <https://doi.org/10.1016/j.jmr.2005.04.005>

SUPPORTING INFORMATION

Additional supporting information may be found in the online version of the article at the publisher's website.

How to cite this article: Wermter FC, Bock C, Dreher W. Characterization of amine proton exchange for analyzing the specificity and intensity of the CEST effect: from humans to fish. *NMR in Biomedicine*. 2021;e4622. doi:10.1002/nbm.4622